Available online at www.sciencedirect.com
SCIENCE DIRECT
Journal of Catalysis 236 (2005) 112–121
JOURNAL OF CATALYSIS
www.elsevier.com/locate/jcat

Structure-sensitivity of hydrodesulfurization of 4,6-dimethyldibenzothiophene over silica-supported nickel phosphide catalysts

Yuying Shu, Yong-Kul Lee, S. Ted Oyama *

Environmental Catalysis and Nanomaterials Laboratory, Department of Chemical Engineering (0211), Virginia Polytechnic Institute and State University, Blacksburg, VA 24061, USA

Received 3 June 2005; revised 21 August 2005; accepted 24 August 2005

Available online 20 October 2005

Abstract

The effect of surface area on the hydrodesulfurization (HDS) of 4,6-dimethyldibenzothiophene (4,6-DMDBT) was studied on a series of supported nickel phosphide catalysts of low (Ni_2P/SiO_2-L, 96 $m^2\,g^{-1}$), medium (Ni_2P/SiO_2-M, 133 $m^2\,g^{-1}$), and high (Ni_2P/SiO_2-H, 208 $m^2\,g^{-1}$) specific surface areas. The activity was based on 240 μmol of active sites (as measured by CO chemisorption) loaded in the reactor and was measured at 573–643 K and 3.1 MPa. The best catalyst, Ni_2P/SiO_2-H, gave a steady-state conversion of 99+% at 613 K, which was higher than that of the Ni_2P/SiO_2-M catalyst with a conversion of 94% or the Ni_2P/SiO_2-L catalyst with a conversion of 76%. The order (H > M > L) correlated with the dispersion of the catalysts as measured from the respective CO uptakes for the samples (125 vs. 99 vs. 59 $\mu mol\,g^{-1}$), and the Ni_2P crystallite size as determined from X-ray diffraction (XRD) line-broadening measurements (6.5 vs. 7.8 vs. 10.1 nm). The higher surface area catalysts gave more of the 3-(3′-methylcyclohexyl)toluene and 3,3′-dimethylbicyclohexyl products, indicating that the small Ni_2P crystallites favor desulfurization by the hydrogenation route. Increasing the reaction temperature from 573 to 643 K enhanced the HDS activities and at the same time gave more 3,3′-dimethylbiphenyl product, indicating that high reaction temperatures favor the direct desulfurization route. Extended X-ray absorption fine structure (EXAFS) and elemental analysis measurements showed that the nickel phosphide was partially sulfided and probably formed a surface phosphosulfide phase in the course of the HDS reaction. The superior activity and stability of the Ni_2P/SiO_2-H catalyst was likely due to the better accessibility of the hindered 4,6-DMDBT molecule to the catalyst surface. The HDS reaction for this molecule is structure-sensitive.

Keywords: Hydrodesulfurization; 4,6-Dimethyldibenzothiophene; Ni_2P/SiO_2; SiO_2; BET; CO uptake; XRD; EXAFS

1. Introduction

Interest in the development of novel catalysts for ultra-deep hydrodesulfurization (HDS) has accelerated throughout the world by the need to meet stringent environmental regulations [1,2] for ultra-low-sulfur (<10 ppm) gasoline, diesel fuels, and jet fuels [2]. The chief challenge in ultra-deep HDS is to remove sulfur from unreactive sulfur compounds, of which the family of dibenzothiophene molecules alkylated next to the sulfur atom is characteristic. A representative member of this family is 4,6-dimethyldibenzothiophene (4,6-DMDBT), which has been used extensively as a model compound [2–4].

Transition metal phosphides have recently been reported as new types of high-activity hydroprocessing catalysts that have substantial promise as next-generation catalysts [5–14]. The nature, structure, and synthesis of phosphides have been described previously [15]. Basically, the phosphides have physical properties similar to those of ordinary metallic compounds, such as carbides and nitrides. Thus they are good conductors of heat and electricity, are hard and strong, and have high thermal and chemical stability. Among the phosphides, nickel phosphide (Ni_2P) has been found to be the most active [5,13], and several articles have described its HDS properties for treating thiophene [9,10] and dibenzothiophene (DBT) [11–13]. For ex-

* Corresponding author. Fax: +1 540 231 5022.
E-mail address: oyama@vt.edu (S.T. Oyama).

0021-9517/$ – see front matter
doi:10.1016/j.jcat.2005.08.015

ample, an optimized Ni_2P catalyst supported on a low-surface area SiO_2 gave a DBT conversion of 100%, much higher than that of a commercial Ni–Mo–S/γ-Al_2O_3 with an HDS conversion of 76% [11]. But this same catalyst had lower activity for the HDS of 4,6-DMDBT, with a steady-state conversion also of 76% [16].

The present study used silicas of different surface areas as supports for nickel phosphide, to examine the effect of particle size on the stability and reactivity of the catalysts. The catalysts using silicas of low (102 $m^2\,g^{-1}$), medium (201 $m^2\,g^{-1}$), and high (333 $m^2\,g^{-1}$) specific surface areas are denoted by Ni_2P/SiO_2-L, Ni_2P/SiO_2-M, and Ni_2P/SiO_2-H, respectively. Silica was chosen as the support because it is inert and provides an opportunity to observe the effect of nickel phosphide particle size on catalytic HDS behavior. The reaction studies were carried out with a model liquid feed containing 500 ppm sulfur as 4,6-DMDBT, 3000 ppm sulfur as dimethyl disulfide, and 200 ppm nitrogen as quinoline. As will be discussed, the HDS of 4,6-DMDBT is a structure-sensitive reaction.

2. Experimental

2.1. Materials

The supports used in this study were fumed silicas with different surface areas (Cabosil, L-90, M-5, EH-5). The chemicals used in the synthesis of the catalysts were $Ni(NO_3)_2 \cdot 6H_2O$ (Alfa Aesar, 99%) and $(NH_4)_2HPO_4$ (Aldrich, 99%). The chemicals used in the reactivity study were 4,6-dimethyldibenzothiophene (Acros Organics, 95%), dimethyl disulfide (Acros Organics, 99%), quinoline (Aldrich, 98%), tetralin (Aldrich, 97%), *n*-octane (Acros Organics, 99%), and *n*-tridecane (Alfa Aesar, 99%). The gases used were H_2 (Airco, Grade 5, 99.99%), He (Airco, Grade 5, 99.99%), CO (Linde Research Grade, 99.97%), and 0.5% O_2/He (Airco, UHP Grade, 99.99%). The reference standards used in the EXAFS study were Ni_2P (Cerac, 99.5%), NiO (Cerac, 99%), Ni (Aldrich, 99.8%), NiS_2 (Aldrich, 99.98%), and NiS (Cerac, 99.9%).

2.2. Synthesis

A series of silica-supported nickel phosphide catalysts were prepared by means of temperature-programmed reduction (TPR), following procedures reported previously [11,12]. Briefly, synthesis of the catalysts involved two stages. First, solutions of nickel phosphate precursors were prepared by dissolving nickel nitrate with ammonium phosphate in distilled water, and these solutions were used to impregnate silica by the incipient wetness method. The obtained samples were dried and calcined at 773 K for 6 h, then ground with a mortar and pestle, pelletized with a press (Carver, Model C), and sieved to particles of 650–1180 μm diameter (16/20 mesh). Second, the solid phosphates were reduced to phosphides from room temperature (RT) to 623 K at 3.6 K min^{-1} and from 623 to 853 K at 1 K min^{-1} in flowing H_2 [1000 cm^3 (NTP) $min^{-1}\,g^{-1}$]. The samples were kept at 853 K for 0.5 h, followed by cooling to RT under He flow [100 cm^3 (NTP) min^{-1}], and then passivated at RT in a 0.5% O_2/He for 4 h. The Ni molar loading was 1.156 mmol g^{-1} (mmol per g of support), corresponding to a weight loading of 7.9% with an initial Ni/P ratio of 1/2; the corresponding samples are denoted by Ni_2P/SiO_2-L, M, and H, where L, M, and H indicate low, medium, and high specific surface areas of the silica support, respectively. These supports were Aerosil samples (Cabosil L-90, M-5, EH-5).

2.3. Characterization

Irreversible CO uptake measurements were used to titrate the surface nickel atoms and to provide an estimate of the active Ni_2P sites on the catalysts. Uptakes were obtained after passivation and rereduction. Usually, 0.2 g of a passivated sample was loaded into a quartz reactor and pretreated in H_2 at 723 K for 3 h. After cooling in He, pulses of CO in a He carrier at 43.4 μmol s^{-1} [65 cm^3 (NTP) min^{-1}] were injected at RT through a sampling valve, and the mass 28 (CO) signal was monitored with a mass spectrometer. CO uptake was calculated by measuring the decrease in the peak areas caused by adsorption in comparison with the area of a calibrated volume (19.5 μmol).

Surface areas of the samples were obtained by the BET method based on adsorption isotherms at liquid nitrogen temperature, using a value of 0.162 nm^2 for the cross-sectional area of a N_2 molecule. The measurements were performed in a volumetric adsorption unit (Micromeritics ASAP 2000).

X-ray diffraction (XRD) patterns of both the fresh and spent samples were obtained with a Scintag XDS-2000 powder diffractometer operated at 45 kV and 40 mA, using Cu-K_α monochromatized radiation ($\lambda = 0.154178$ nm). Crystallite sizes were calculated from the XRD peak line widths using the Scherrer equation, $D_c = K\lambda/\beta\cos(\theta)$, where K is a constant taken as 0.9, λ is the wavelength of the X-ray radiation, β is the peak width in radians at half-maximum corrected for instrumental broadening (0.1°), and 2θ is the Bragg angle of the reflection [17].

Elemental analysis was carried out with an inductively coupled plasma atomic emission spectrometer (Spectroflame FTMO A85D; Spectro Analytical Instruments) on samples that had been dissolved in aqua regia in a microwave digester (EthosPlus, Milestone). The nickel and phosphorus signals were calibrated with a solution of nickel nitrate and ammonium phosphate.

Equilibrium calculations were carried out using the CHETAH program (ASTM International, West Conshohocken, PA). Multiple reaction equilibria were obtained by simultaneous solution of equilibrium equations.

To determine changes in the structures of the Ni_2P/SiO_2 catalysts with variation of SiO_2 supports and reactions, the samples were examined using extended X-ray absorption fine structure (EXAFS) analysis. Ni K-edge EXAFS spectra were obtained for both the fresh and spent samples. The fresh samples were pretreated in H_2 flow at 723 K, whereas the spent samples were removed from the reactors in oil without contact with ambient air, loaded in glass reactors, washed with

hexane, dried, and treated in He flow at 623 K. Both the freshly prepared samples and the spent samples were transferred to glass cells with Kapton windows and were sealed by glass-blowing without exposure to the atmosphere. The measurements were made in transmission mode at the X18B beamline in Brookhaven National Laboratory with a 2.5 GeV ring energy and 400-mA ring current. For the EXAFS analysis, comparisons were made with several bulk standards, including Ni_2P (Cerac, 99.5%), NiO (Cerac, 99%), Ni (Aldrich, 99.8%), NiS_2 (Aldrich, 99.98%), and NiS (Cerac, 99.9%). The obtained EXAFS data were analyzed using the WinXAS97 software package. A two-polynomial-fit function was used for background subtraction in the entire spectral range. The k^3-weighted EXAFS function was Fourier-transformed into R-space using a k-range of 2.5–14 $Å^{-1}$.

2.4. Reactivity studies

Hydrotreating activities of the samples were tested in a three-phase, packed-bed reactor operated at 3.1 MPa and 573–643 K with a model feed liquid containing 500 ppm sulfur as 4,6-DMDBT, 3000 ppm sulfur as dimethyl disulfide, 200 ppm nitrogen as quinoline, 1 wt% tetralin, 0.5 wt% n-octane as an internal standard, and the balance n-tridecane. The schematic of the testing system was described previously [18]. Briefly, the testing unit comprised three parallel reactors immersed in a fluidized sand bath (Techne, model SBL-2) with a temperature controller (Omega, model 6015 K). The reactors were 19-mm o.d./16-mm i.d. 316 stainless steel tubes with central thermocouples to monitor the temperature of the catalyst. The catalysts were in the form of pellets (16/20 mesh) and were supported between quartz wool plugs in a 13-mm i.d. 316 stainless steel basket. The hydrogen flow rate was set to 150 $cm^3\,min^{-1}$ with a mass flow controller (Brooks, model 5850E), and the feed liquid was injected by a high-pressure liquid pump (LDC Analytical, model NCI 11D5) at a flow rate of 5 $cm^3\,h^{-1}$. Quantities of catalysts loaded in the reactors corresponded to the same amount of CO uptake (240 μmol). The LHSVs for the L, M, and H catalyst were 0.47, 0.79, and 1.0 h^{-1}, respectively, based on catalyst amounts of 3.89, 2.32, and 1.84 g and an apparent catalyst density of 0.37 $g\,cm^{-3}$. The passivated catalysts were rereduced under H_2 at 723 K for 3 h before the feed liquid was introduced into the reactors. Hydrotreating products were collected every few hours in sealed septum vials and analyzed by a gas chromatograph (Hewlett–Packard, 5890A) equipped with a 0.32-mm i.d. × 50-m fused silica capillary column (CPSIL-5CB; Chrompack) and a flame ionization detector.

3. Results and discussion

3.1. BET and CO chemisorption

The BET specific surface areas (S_g) and CO chemisorption uptakes of the various silica supports and silica-supported nickel phosphide samples are given in Table 1. Results are shown for freshly reduced samples (fresh) and used samples (spent) after reaction for 100 h. The BET surface areas of the fresh SiO_2-L, SiO_2-M, and SiO_2-H supports were 102, 201, and 333 $m^2\,g^{-1}$, respectively. After the introduction of nickel phosphides on the supports, the BET surface areas decreased to 96, 133, and 208 $m^2\,g^{-1}$, respectively. The higher-surface area supports, SiO_2-M and SiO_2-H, lost proportionally more area, probably because their smaller particles were more prone to sintering by the high-temperature (853 K) treatment used in the catalyst synthesis. In addition, more of their intraparticle volume may have been filled by the nickel phosphide phase. The BET areas of the spent samples also decreased further, but only moderately, to 78, 112, and 174 $m^2\,g^{-1}$.

Table 1
Characterization of the silica-supported nickel phosphide samples

Samples	Condition	BET surface area S_g ($m^2\,g^{-1}$)	CO uptake (μmol g^{-1})	D_c (nm)
SiO_2-L	–	102	0	–
SiO_2-M	–	201	0	–
SiO_2-H	–	333	0	–
Ni_2P/SiO_2-L	Fresh	96	59	10.1
	Spent	78	40	–
Ni_2P/SiO_2-M	Fresh	133	99	7.8
	Spent	112	73	–
Ni_2P/SiO_2-H	Fresh	208	125	6.5
	Spent	174	102	–

The CO chemisorption uptakes for the fresh samples increased substantially with increasing surface area of the silica support. CO uptake was 59 μmol g^{-1} for the Ni_2P/SiO_2-L sample, 99 μmol g^{-1} for the Ni_2P/SiO_2-M sample, and 125 μmol g^{-1} for the Ni_2P/SiO_2-H sample (Table 1). These results demonstrate that the higher-surface area supports gave rise to greater dispersion of the Ni_2P phase. Consistent with this, the crystallite sizes (D_c) calculated from the Scherrer equation [$D_c = K\lambda/\beta\cos(\theta)$] [17] became smaller with increasing silica surface area, from 10.1 to 7.8 and then to 6.5 nm (Table 1).

3.2. XRD and elemental analysis

The XRD patterns of the fresh Ni_2P/SiO_2 samples prepared from the different silica supports are presented in Fig. 1. The patterns all show a broad feature at $2\theta \sim 22°$ due to the amorphous silica supports. At higher angles, peaks due to Ni_2P are visible for all samples. The assignment of Ni_2P is based on powder diffraction file (PDF) 3–953 [Fig. 1d]. The XRD peaks for Ni_2P became less sharp and intense with increasing surface area of the silica, consistent with the decreased size of the Ni_2P crystallites on the high-surface area supports.

The XRD patterns for the spent samples with the different silica supports were also obtained and are shown in Fig. 2. The figure shows a distinct decrease in the Ni_2P peak intensity after reaction for the low-surface area samples. In contrast, there was no change in pattern and intensity for the Ni_2P/SiO_2-H sample, indicating that the smaller Ni_2P particles were stable at the hydrotreating conditions on this high-surface area silica support.

The elemental analysis results for the various samples are listed in Table 2. All of the Ni_2P/SiO_2 samples were prepared at a Ni molar loading of 1.156 mmol g^{-1} (7.9 wt% Ni_2P) with

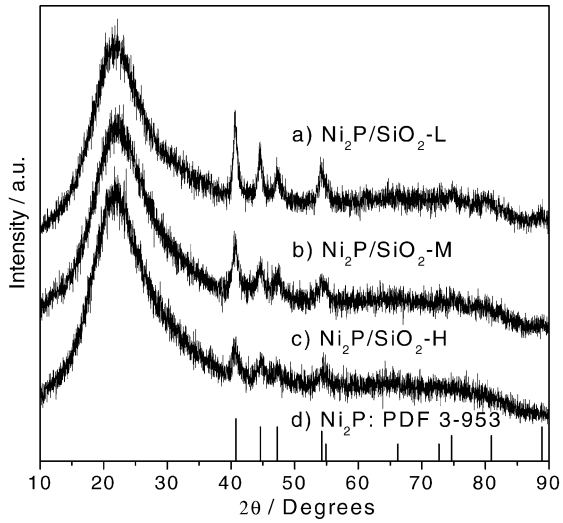

Fig. 1. X-ray diffraction patterns of the fresh Ni_2P/SiO_2 samples, (a) Ni_2P/SiO_2-L, (b) Ni_2P/SiO_2-M, (c) Ni_2P/SiO_2-H, and (d) reference Ni_2P (PDF 3-953).

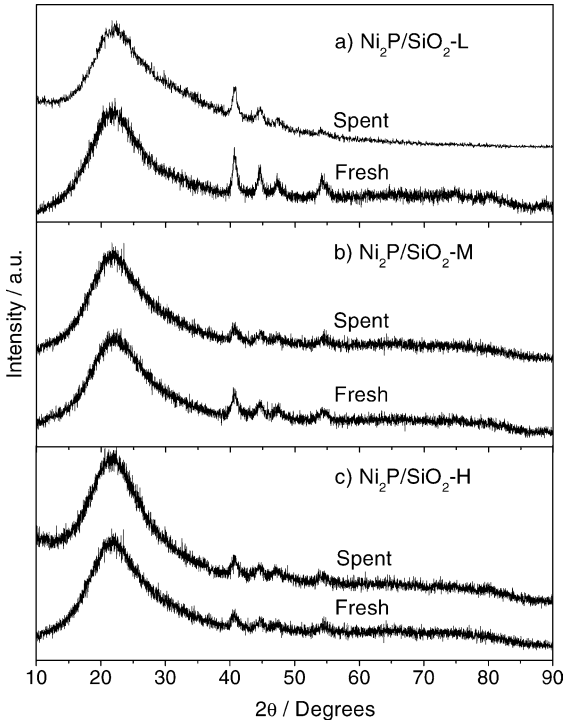

Fig. 2. Comparison of X-ray diffraction patterns for the fresh and spent Ni_2P/SiO_2 samples, (a) Ni_2P/SiO_2-L, (b) Ni_2P/SiO_2-M, and (c) Ni_2P/SiO_2-H.

an initial Ni/P ratio of 1/2, a four-fold excess of P over the stoichiometric value of 1/0.5. Results are given for the freshly reduced samples (fresh) and the used samples (spent) after reaction for 100 h. For the Ni_2P/SiO_2-H sample, the elemental analysis of the precursor phosphate material (calcined) is also reported. In all cases, the freshly prepared Ni_2P/SiO_2 samples had lower phosphorus content than the initial value, with Ni/P ratios ranging from 1/0.84 to 1/1.04, higher than the expected stoichiometric value of 1/0.50 for Ni_2P. The substantial excess of P was probably located mainly on the support surface, because the XRD patterns showed the presence of Ni_2P as the only phosphide phase in the fresh sample. The Ni/P ratio indicated that more phosphorus was retained on the medium- and high-surface area samples. As for the calcined sample, the Ni/P ratio was 1/2.01, very close to the initial amount of 1/2, indicating that the phosphorus loss occurred not during the calcination stage, but rather during the reduction step of the preparation. The elemental analysis also demonstrated a distinct decrease in phosphorus content for all of the spent samples, especially for the silica-supported samples with low and medium surface areas. The decrease in the amount of P was 43% for SiO_2-L, 38% for SiO_2-M, and 22% for SiO_2-H, as calculated from the corresponding Ni/P ratios of 1/0.48, 1/0.62, and 1/0.81, respectively. These results are consistent with the greater stability of the Ni_2P on the high-surface area sample.

Table 2
Elemental analysis of the silica-supported nickel phosphide samples

Sample	Condition	Composition (wt%)			Molar ratio	
		Ni	P	S	Ni/P	Ni/S
Ni_2P/SiO_2-L	Fresh	4.97	2.20	–	1/0.84	–
	Spent	3.99	1.57	0.370	1/0.48	1/0.170
Ni_2P/SiO_2-M	Fresh	5.13	2.64	–	1/0.98	–
	Spent	4.91	1.60	0.339	1/0.62	1/0.126
Ni_2P/SiO_2-H	Calcined	4.38	4.65	–	1/2.01	–
	Fresh	4.64	2.54	–	1/1.04	–
	Spent	4.21	1.79	0.334	1/0.81	1/0.145

Sulfur content determinations were also made by elemental analysis of the spent samples; the results are given in the last column of Table 2 as metal/S molar ratios. In all cases, some sulfur was taken up by the catalysts, with Ni/S ratios ranging from 1/0.126 to 1/0.170. The location of the sulfur is not completely ascertained; some sulfur may have resided on the support in the form of adsorbed organic moieties, and some may have been located on the catalytic phase. As demonstrated by the Ni *K*-edge EXAFS results (reported later in this paper), some of the sulfur likely interacted with the surface of the nickel phosphide crystallites to form a phosphosulfide phase. The phosphosulfide is formed on the surface, because the XRD results indicate that the bulk of the crystallites remained Ni_2P. Moreover, the surface is not a pure sulfide, because phosphorus was still predominant on the Ni_2P/SiO_2, and the reactivity of nickel sulfide is known to be poor [19].

3.3. Reactivity studies

A model feed containing 500 ppm sulfur as 4,6-DMDBT, 3000 ppm sulfur as dimethyl disulfide, 200 ppm nitrogen as quinoline, 1 wt% tetralin, and 0.5 wt% *n*-octane in *n*-tridecane was used to test the HDS, hydrodenitrogenation (HDN), dehydrogenation (DeHYD), and hydrogenation (HYD) activities of the various Ni_2P/SiO_2 catalysts. Fig. 3 illustrates the time course of HDS activities for the various Ni_2P/SiO_2 catalysts at 613 K and 3.1 MPa. The initial 4,6-DMDBT conversions were uniformly high for all of the samples but declined significantly for the Ni_2P/SiO_2-L, declined slightly for the Ni_2P/SiO_2-M, and actually grew for the Ni_2P/SiO_2-H. The Ni_2P/SiO_2-H cat-

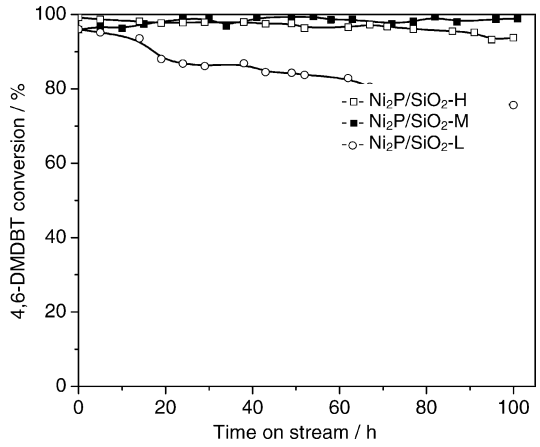

Fig. 3. Conversions of 4,6-DMDBT HDS as a function of time on stream at 613 K and 3.1 MPa over Ni_2P/SiO_2-L, Ni_2P/SiO_2-M, and Ni_2P/SiO_2-H catalysts.

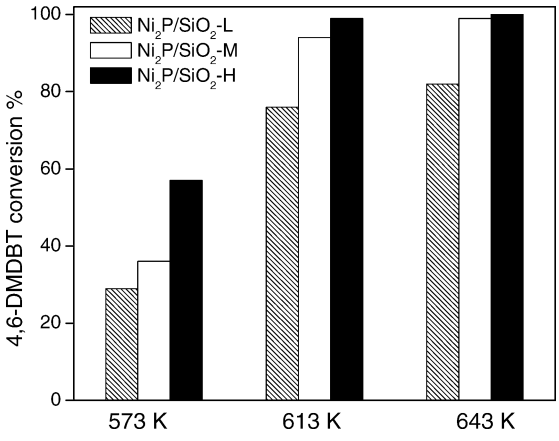

Fig. 4. Activity comparison of 4,6-DMDBT HDS for Ni_2P/SiO_2-L, Ni_2P/SiO_2-M, and Ni_2P/SiO_2-H catalysts. The reaction is carried out at 573, 613, and 643 K, respectively.

alyst gave the highest 4,6-DMDBT conversion (99+%), even after 100 h of reaction; the Ni_2P/SiO_2-M catalyst gave an intermediate conversion (94%), and the Ni_2P/SiO_2-L catalyst gave the lowest conversion (76%). The Ni_2P/SiO_2-L catalyst showed some decline in activity over time. The deactivation of the lower-surface area catalyst is likely due to the loss of active sites, as revealed by the chemisorption data (Table 1). Table 1 shows a decrease from 59 to 40 μmol g^{-1} (32%) for Ni_2P/SiO_2-L and from 99 to 73 μmol g^{-1} (26%) for Ni_2P/SiO_2-M. Ni_2P/SiO_2-H also lost some chemisorption sites, from 125 to 102 μmol g^{-1}, but this loss was less (18%) than that in the other samples. The loss of sites may be related to excessive sulfidation of the catalysts, which was the highest for the Ni_2P/SiO_2-L catalyst. Overall, in terms of activity and stability, the Ni_2P/SiO_2-H catalyst was superior to the low- and medium-surface area catalysts.

A comparison of the HDS activity for the various Ni_2P/SiO_2 catalysts at different reaction temperatures of 573, 613, and 643 K is given in Fig. 4. The 4,6-DMDBT conversion increased with increase in the reaction temperatures. The apparent activation energies for reaction were 25.8 kJ mol^{-1} for Ni_2P/SiO_2-H, 46.2 kJ mol^{-1} for Ni_2P/SiO_2-M, and 47.5 kJ mol^{-1} for Ni_2P/SiO_2-L. The substantially lower activation energy for the Ni_2P/SiO_2-H sample was related to its higher reactivity compared with the Ni_2P/SiO_2-M and Ni_2P/SiO_2-L samples.

The conversions and product distributions at 613 K and 3.1 MPa after 100 h are summarized in Table 3. The table lists the reactant in the first column, the reaction type in the second column, and a set of conversions and selectivities for the samples in subsequent columns. The selectivities add up to 100% for each reaction type, and mass balances were 100 ± 5%. As discussed earlier, the high-surface area silica-supported catalyst, Ni_2P/SiO_2-H, displayed the highest activity, with a 4,6-DMDBT conversion of 99+%, substantially higher than the 94% conversion in Ni_2P/SiO_2-M and the 76% conversion in Ni_2P/SiO_2-L. The HDS activity of the Ni_2P/SiO_2-H catalyst was also much higher than that of a commercial Ni–Mo–S/γ-Al_2O_3 catalyst, which gave a 4,6-DMDBT conversion of 68% under the same reaction conditions [16]. The Ni_2P/SiO_2-L catalyst was previously reported to be the most active phosphide catalyst for the desulfurization of DBT [5,20]. In all cases the comparisons are based on 240 μmol of sites loaded in the reactor, with the sites counted by CO chemisorption for the phosphides and low-temperature O_2 chemisorption for the commercial sulfide. Thus this comparison demonstrates that the intrinsic activity of the high-surface area catalyst was the best and

Table 3
The conversions and selectivities of the silica-supported nickel phosphides at 613 K and 3.1 MPa after 100 h on stream

Reactants	Type	Conversion (%)			Product	Selectivity (%)		
		Ni_2P/SiO_2-L	Ni_2P/SiO_2-M	Ni_2P/SiO_2-H		Ni_2P/SiO_2-L	Ni_2P/SiO_2-M	Ni_2P/SiO_2-H
4,6-DMDBT	HDS	76	94	99	3,3′-Dimethylbiphenyl	44	15	12
					3-(3′-Methylcyclohexyl)toluene	42	54	53
					3,3′-Dimethylbicyclohexyl	14	31	35
Quinoline	HDN	92	100	100	Propylcyclohexane	52	64	74
					Propylbenzene	41	36	26
	HYD	6	0	0	Orthopropylaniline	4	0	0
					5,6,7,8-Tetrahydroquinoline	2	0	0
					1,2,3,4-Tetrahydroquinoline	1	0	0
Tetralin	DeHYD	23	7	6	Naphthalene	69	28	25
	HYD	10	17	20	*Trans*-decalin	21	46	49
					Cis-decalin	10	26	26

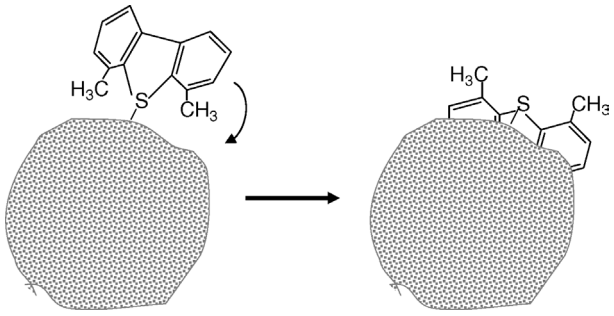

Fig. 5. Schematic of interaction of 4,6-DMDBT on small particles of Ni_2P.

much higher than that of the low- and medium-surface area catalysts. The reason for this is related to the higher dispersion and stability of the fine particles of Ni_2P, which can maintain their structure at reaction conditions.

Three major products are formed from 4,6-DMDBT conversion on the Ni_2P/SiO_2-L, Ni_2P/SiO_2-M, and Ni_2P/SiO_2-H catalysts: 3,3′-dimethylbiphenyl (DMBP), 3-(3′-methylcyclohexyl)toluene (MCHT), and 3,3-dimethylbicyclohexyl (DMBCH). According to published literature [21–25], the DMBP can be considered to be formed by a direct desulfurization (DDS) pathway, whereas the MCHT and DMBCH products from a hydrogenation (HYD) pathway. As will be seen, this is reasonable as secondary hydrogenation and dehydrogenation reactions are not favored at reaction conditions because of strong adsorption by the sulfur-containing molecules. Compared to the Ni_2P/SiO_2-L catalyst, the Ni_2P/SiO_2-H catalyst gave a lower DMBP selectivity of 12% and a higher DMBCH selectivity of 35%, indicating that it favors the hydrogenation pathway. This will be discussed below.

The likely reason for the differences in selectivity between catalysts is that 4,6-DMDBT is a highly hindered molecule and as such can interact more easily with the smaller particles. A possible scenario for this is depicted in Fig. 5. The 4,6-DMDBT compound first interacts with a small particle through the S-atom, which provides the strongest bond to a Ni center. Direct desulfurization could occur at this point, but the rate of this reaction is low. Instead, because of the small particle size (exaggerated in the figure), the adsorbed molecule can swing around to cause interaction of the phenyl rings with the surface. This leads to hydrogenation and eventual desulfurization. The sequence constitutes a two-point mechanism, requiring interaction of the 4,6-DMDBT molecule with the surface through the S-atom and at least one of the phenyl rings. The mechanism is not expected to be readily operable in the lower-surface area materials with larger particles; for these samples, the number of sites capable of interacting with the sulfur atom will be lower, and the flatness of the surface will inhibit rotation of the compound to allow interaction of the phenyl rings with the surface. The finding that DDS is favored on these samples is consistent with this picture. As will be seen, the model is also consistent with the results of the tetralin reaction (discussed later in the paper). The larger particles with fewer sites for adsorption of 4,6-DMDBT will have more bare flat surfaces, permitting the adsorption of other molecules that normally would be inhibited

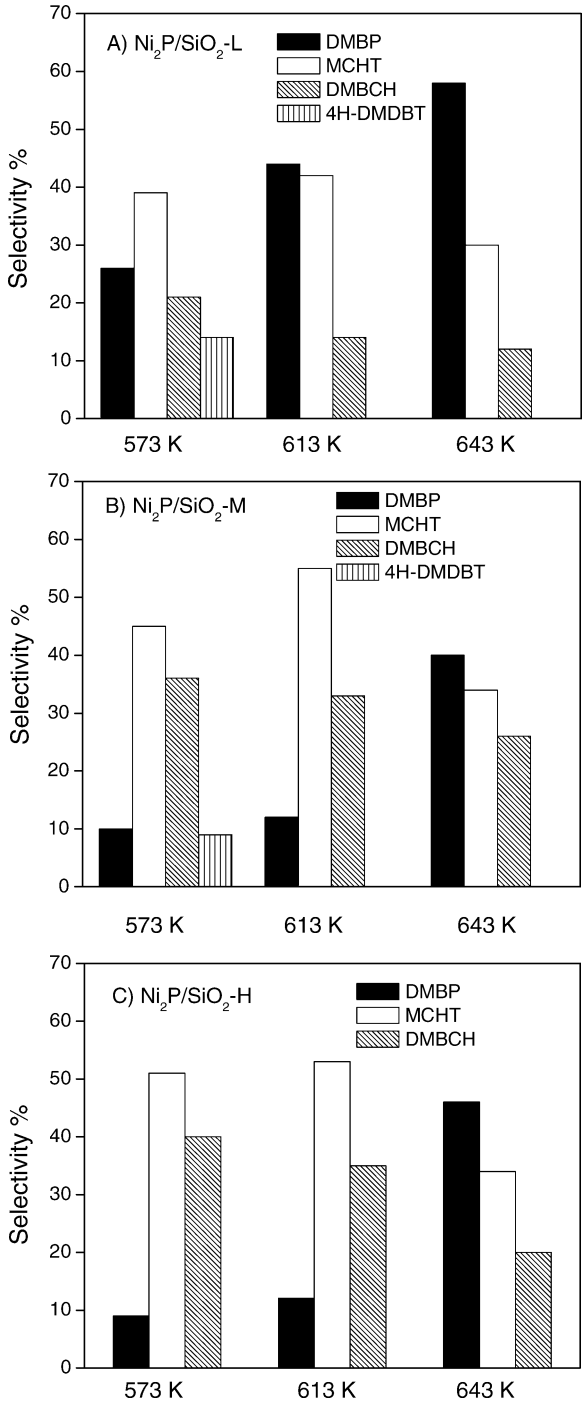

Fig. 6. Product distribution of 4,6-DMDBT HDS for (A) Ni_2P/SiO_2-L, (B) Ni_2P/SiO_2-M, and (C) Ni_2P/SiO_2-H catalysts. The products are 3,3′-dimethylbiphenyl (DMBP), 3-(3′-methylcyclohexyl)toluene (MCHT), 3,3′-dimethylbicyclohexyl (DMBCH), and 1,2,3,4-tetrahydro-4,6-dimethyldibenzothiophene (4H-DMDBT), at 573, 613, and 643 K, respectively.

by the presence of 4,6-DMDBT. This results in higher tetralin conversions for the lower-surface area materials.

The 4,6-DMDBT HDS product distributions for the Ni_2P/SiO_2-L, Ni_2P/SiO_2-M, and Ni_2P/SiO_2-H catalysts at 573, 613, and 643 K are shown as bar charts in Figs. 6A, 6B, and 6C, respectively. Three distinct features can be observed. First, at the lowest temperature of 573 K, there is an additional prod-

Table 4
The tetralin conversions and selectivities of the silica-supported nickel phosphides at the different temperatures

Reac. temp. (K)	Conversion of tetralin (%)			Product	Selectivity (%)		
	Ni_2P/SiO_2-L	Ni_2P/SiO_2-M	Ni_2P/SiO_2-H		Ni_2P/SiO_2-L	Ni_2P/SiO_2-M	Ni_2P/SiO_2-H
573	10	7	9	Naphthalene	70	31	27
				Trans-decalin	20	44	49
				Cis-decalin	10	25	24
613	33	24	26	Naphthalene	69	28	25
				Trans-decalin	21	46	49
				Cis-decalin	10	26	26
643	48	45	46	Naphthalene	82	62	87
				Trans-decalin	10	25	9
				Cis-decalin	8	13	4

uct for the Ni_2P/SiO_2-L and Ni_2P/SiO_2-M catalysts formed besides the three obtained at 613 K (DMBP, MCHT, and DMBCH). The additional product is 1,2,3,4-tetrahydro-4,6-dimethyldibenzothiophene (4H-DMDBT). The appearance of 4H-DMDBT is due to the low conversion at 573 K, which allows observation of hydrogenated precursor species in the sequential hydrogenation pathway before desulfurization. Second, at the highest temperature of 643 K, the product DMBP grew and became predominant for all of the Ni_2P/SiO_2 catalysts. The reason for this is thermodynamic in origin, because aromatic compounds are favored at high temperatures. Third, regardless of the reaction temperature, the Ni_2P/SiO_2-L catalyst had substantially higher DMBP selectivity than the Ni_2P/SiO_2-M and Ni_2P/SiO_2-H catalysts, indicating that direct desulfurization is favored for this low-surface area catalyst. As discussed earlier, this was due to the inability of 4,6-DMDBT to interact through both the S-atom and the phenyl rings on the flatter surfaces and to undergo hydrogenation. It should be remembered, however, that the DDS pathway is slow, and 4,6-DMDBT conversion is not high on the Ni_2P/SiO_2-L catalyst.

Quinoline can react to form HDN and HYD products; the corresponding two conversions are also given in Table 3. The products are classified as denitrogenated compounds (propylcyclohexane, propylbenzene) and hydrogenated molecules (1,2,3,4-tetrahydroquinoline, 5,6,7,8-tetrahydroquinoline, orthopropylaniline). As can be seen, both the Ni_2P/SiO_2-M and Ni_2P/SiO_2-H catalysts showed superior ability for nitrogen removal, with an HDN conversion of 100%, higher than the 92% demonstrated by the Ni_2P/SiO_2-L catalyst. The product distribution shows that propylcyclohexane selectivity increased distinctly with increasing surface area of the supports. The dominant formation of propylcyclohexane implies that hydrogenation of aromatic rings occurred before nitrogen removal.

The main products of the tetralin reaction were naphthalene formed from a DeHYD pathway and *cis*- and *trans*-decalin formed from a HYD pathway. Compared with the Ni_2P/SiO_2-L catalyst, the Ni_2P/SiO_2-M and Ni_2P/SiO_2-H catalysts had slightly lower tetralin conversion (24–26% vs. 33%) and lower naphthalene formation (25–28% vs. 69%). The dehydrogenation ability for tetralin conversion at 613 K and 3.1 MPa followed the order Ni_2P/SiO_2-L > Ni_2P/SiO_2-M ∼ Ni_2P/SiO_2-H. A detailed comparison of tetralin conversion and selectivity at the different reaction temperatures is given in Table 4. As shown, at the lowest temperature of 573 K, tetralin conversion was around 10%, whereas at the highest temperature of 643 K, it increased to nearly 50%. As for the product distributions, with increasing reaction temperature from 573 K to 613 K, the selectivity to hydrogenation products of *trans*- and *cis*-decalin decreased and the selectivity to naphthalene increased. These findings are as expected based on the thermodynamics. Fig. 7A shows the relative equilibrium concentrations for the reaction network of tetralin. As expected, because hydrogenation is exothermic, the concentration of hydrogenated products, *cis*- and *trans*-decalin, decreased with increasing temperature, whereas the concentration of the dehydrogenated product, naphthalene, increased with increasing temperature. The concentration of tetralin goes through a maximum because it can be both hydrogenated and dehydrogenated. Fig. 7B shows the calculated selectivities to the products of tetralin reaction. The same figure displays points corresponding to the observed product selectivities on the Ni_2P/SiO_2-L, Ni_2P/SiO_2-M, and Ni_2P/SiO_2-H catalysts. As can be seen, there are discrepancies between the theoretical and experimental quantities, so that the reaction network is not equilibrated. However, there is a trend for the higher surface area materials with the lower conversions to be closer to equilibrium.

It was also distinctive that for each catalyst, the conversion of tetralin was substantially lower than the corresponding conversions for HDS and HDN (Table 3), despite the fact that tetralin is present in considerable excess (10,000 ppm vs. 500 ppm). This finding demonstrates that secondary hydrogenation/dehydrogenation reactions are less important, probably because the aromatic compounds are adsorbed more weakly than the sulfur or nitrogen compounds.

3.4. EXAFS analysis

To characterize the formation of nickel phosphides on the different silica supports and to elucidate the nature of the possible active phases involved in the hydrotreating reaction, both the fresh and spent silica-supported phosphide samples were analyzed by EXAFS spectroscopy (Figs. 8 and 9). Figs. 8A and

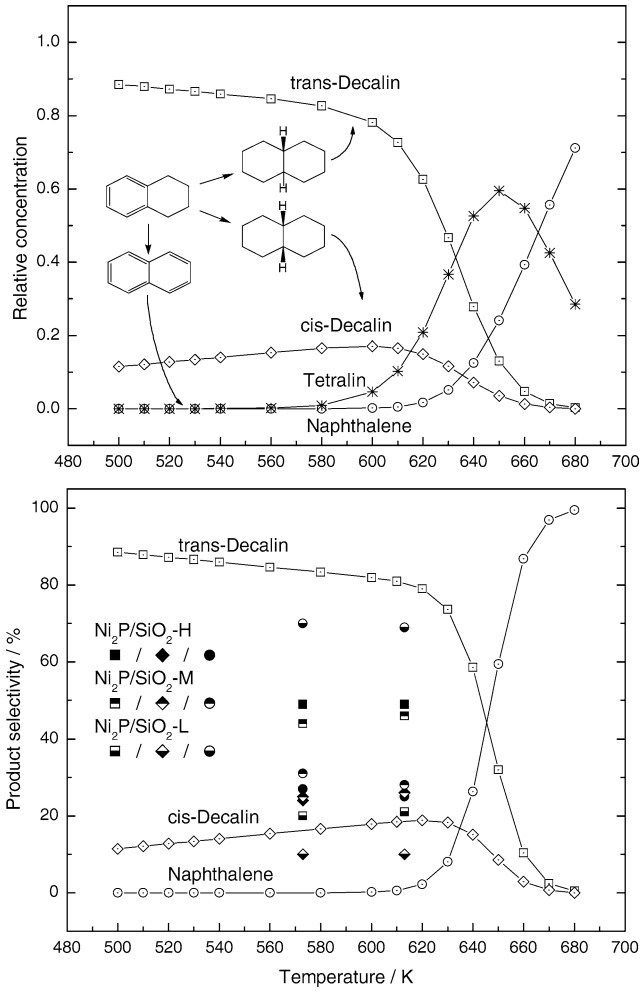

Fig. 7. Equilibrium of tetralin reactions. (A) Concentrations of (✳) tetralin, (□) *trans*-decalin, (◇) *cis*-decalin, and (○) naphthalene. (B) Product selectivities of the reaction. Curves are equilibrium calculations, points are experimental for Ni_2P/SiO_2-L, Ni_2P/SiO_2-M, and Ni_2P/SiO_2-H, (⬒, ⬓, ■) *trans*-decalin, (⬘, ⬙, ◆) *cis*-decalin, and (◓, ◒, ●) naphthalene.

8B show the Fourier-transformed Ni *K*-edge EXAFS spectra of the fresh Ni_2P/SiO_2 samples prepared from the different silica supports, along with some reference standards. The bulk Ni_2P sample shows two main peaks at distances of 0.18 and 0.23 nm, which correspond to Ni–P and Ni–Ni distances [Fig. 8B(a)]. The fresh samples all display two distinct peaks at distances close to those of the Ni_2P standard, indicating that Ni_2P is the predominant phase in these catalysts. There is no indication of the presence of NiO [Fig. 8B(b)], Ni metal [Fig. 8B(c)], or Ni sulfide [Fig. 8B(d)] in these samples.

Ni *K*-edge EXAFS results for both the fresh and spent Ni_2P/SiO_2 samples prepared with the different silica supports are compared in Fig. 9. The features of the fresh Ni_2P/SiO_2 samples (thin lines) and spent samples (bold lines) were different, especially in the Ni–Ni peak region. As can be seen, the Ni–Ni peak shifted to slight lower distances, and the intensity was attenuated. Although not distinct, a broad feature between the Ni–P and Ni–Ni peaks appeared to be formed, because that region displayed a considerable increase in signal intensity. Clearly, there is disruption of the original Ni_2P phase

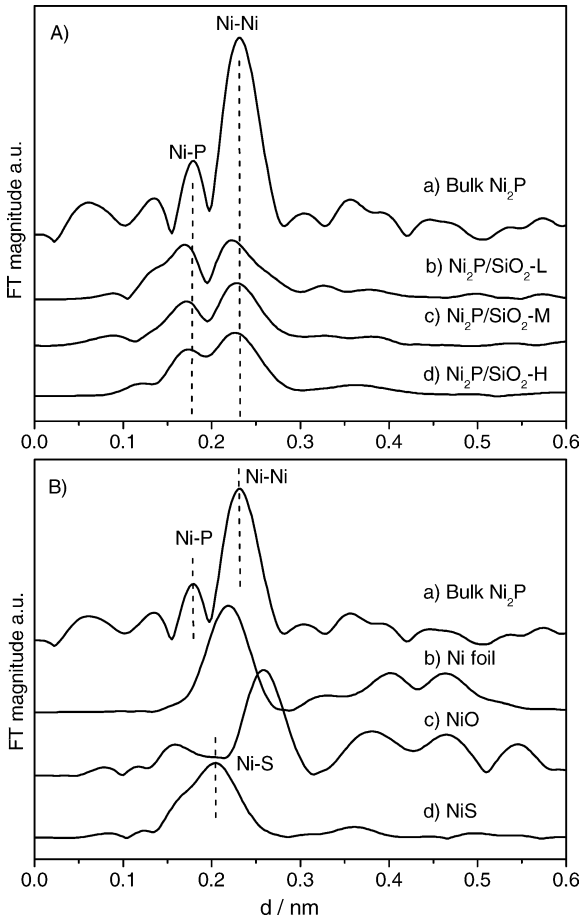

Fig. 8. Nickel *K*-edge EXAFS of the fresh Ni_2P/SiO_2 samples, (A) Ni_2P/SiO_2-L, Ni_2P/SiO_2-M, and Ni_2P/SiO_2-H, (B) Ni_2P, NiO, nickel metal, and NiS references.

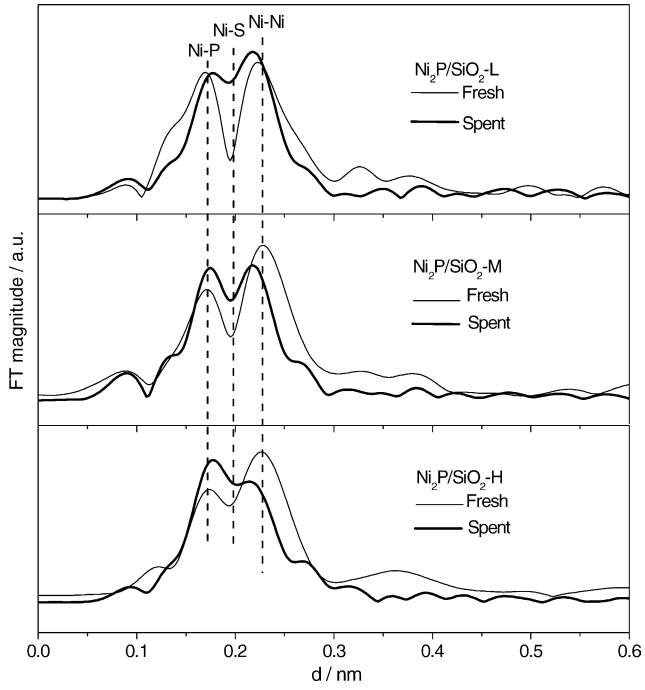

Fig. 9. Nickel *K*-edge EXAFS of the fresh and spent Ni_2P/SiO_2-L, Ni_2P/SiO_2-M, and Ni_2P/SiO_2-H samples.

on the silica supports after the hydrotreating reaction, most likely because of the formation of some phosphorous-deficient Ni phase and/or the formation of sulfur compounds. The shift of the peaks to lower distance, in the direction of Ni metal, would be consistent with this change in composition. The broad, indistinct signal falls exactly in the region of Ni–S linkages, as shown by the spectra of the sulfide standard [Fig. 8B(d)]. Thus, the active phase for the nickel phosphide catalysts is likely to be a Ni–P–S layer on top of Ni_2P crystallites. The presence of small amounts of sulfur was already demonstrated by the elemental analysis results.

3.5. Comparison of different silica as supports for Ni_2P

The different silica supports with low, medium, and high specific surface areas were used to prepare the Ni_2P catalysts at the same molar loading of 1.156 mmol g^{-1} and a Ni/P ratio of 1/2. The Ni_2P/SiO_2-H catalyst exhibited the highest activity and stability compared with the Ni_2P/SiO_2-M and Ni_2P/SiO_2-L catalysts (Table 3; HDS conversions 99+% vs. 94% and 76%, respectively). The higher activity for the higher-surface area silica-supported catalyst is likely due to the presence of a stable Ni_2P phase in fine crystallite form. This also gives rise to a greater dispersion, as seen from the higher CO uptake (Table 1; 125 vs. 99 vs. 59 μmol g^{-1}, respectively) and smaller particle size (Table 1; 6.5 vs. 7.8 vs. 10.1 nm, respectively). Because the activity measurements were made on the basis of equal sites loaded in the reactor, the difference in activity must be due to the higher intrinsic reactivity of the sites in the smaller particles. The differences in the supported phases are also demonstrated in the P content of the samples. Specifically, compared with the low-surface area silica-supported catalyst (Ni_2P/SiO_2-L), the high-surface area silica-supported catalyst (Ni_2P/SiO_2-H) retained more phosphorus after reduction (Table 2; Ni/P ratio = 1/1.04 vs. 1/0.84, respectively) and after reaction (Table 2; Ni/P ratio = 1/0.81 vs. 1/0.48, respectively). The smaller crystallites appear to have stronger Ni–P bonding, allowing them to retain more phosphorus, which accounts for their better stability. This is also seen in the lower loss of chemisorption sites during the course of hydrotreating (Table 1). The different silica-supported catalysts also behaved differently in terms of 4,6-DMDBT product distributions, with the smaller Ni_2P crystallites on the higher-surface area support favoring hydrogenation of both 4,6-DMDBT and tetralin.

4. Conclusions

Nickel phosphide supported on different silica supports (SiO_2-L, SiO_2-M, and SiO_2-H) was successfully prepared by the TPR method from the corresponding nickel phosphate, as demonstrated by XRD and EXAFS measurements. The HDS activity of 4,6-DMDBT was studied under simulated industrial conditions of 573–643 K and 3.1 MPa with a model liquid feed containing 500 ppm sulfur as 4,6-DMDBT, 3000 ppm sulfur as dimethyl disulfide, and 200 ppm nitrogen as quinoline. The Ni_2P/SiO_2-H catalyst demonstrated superior HDS and HDN performance and was found to be best for sulfur removal from the tenacious 4,6-DMDBT compound among the silica-supported catalysts tested. The surface area of the silica support was found to have a profound effect on Ni_2P dispersion, Ni_2P/SiO_2 particle size, and 4,6-DMDBT HDS behavior. The Ni_2P/SiO_2-H catalyst at 613 K and 3.1 MPa gave a steady-state 4,6-DMDBT conversion of 99+%, much higher than those of the Ni_2P/SiO_2-M (94%) and Ni_2P/SiO_2-L (76%) catalysts. This is due to the higher dispersion of Ni_2P on the higher-surface area SiO_2 support and the corresponding smaller Ni_2P particles. The stability of this Ni_2P/SiO_2-H catalyst was also excellent, with no deactivation observed in the prolonged 100 h reaction. Compared with Ni_2P/SiO_2-L, the Ni_2P/SiO_2-H catalyst demonstrated lower 3,3′-dimethylbiphenyl (DMBP) selectivity (12%), higher 3-(3′-methylcyclohexyl)toluene (MCHT) selectivity (53%) and higher 3,3′-dimethylbicyclohexyl (DMBCH) selectivity (35%), demonstrating that the relatively smaller Ni_2P crystallites favor the HDS pathway. These findings were further confirmed by comparison of the product distributions among the Ni_2P/SiO_2-L, Ni_2P/SiO_2-M, and Ni_2P/SiO_2-H catalysts. The XRD patterns of the spent samples showed that the bulk structure of Ni_2P was maintained during the course of hydrotreatment. Characterization of the catalysts by EXAFS and elemental analysis measurements before and after reaction indicated that the phosphides underwent a partial sulfidation that led to the formation of a phosphosulfide layer on top of a Ni_2P phase. The excellent performance of the Ni_2P/SiO_2-H catalyst might be related to the higher Ni_2P dispersion, smaller Ni_2P particle size, and better stability of the Ni_2P structure in the HDS course compared with the larger Ni_2P crystallite size in the Ni_2P/SiO_2-L and Ni_2P/SiO_2-M catalysts.

Acknowledgments

This work was supported by the U.S. Department of Energy, Office of Basic Energy Sciences (grant DE-FG02-963414669) and Brookhaven National Laboratory (grant 4513) for using the X18B beamline at the National Synchrotron Light Source.

References

[1] J. Kemsley, Chem. Eng. News 81 (43) (2003) 40.
[2] C. Song, Catal. Today 86 (2003) 211.
[3] D.D. Whitehurst, T. Isoda, I. Mochida, Adv. Catal. 42 (1998) 345.
[4] K.G. Knudsen, B.H. Cooper, B.H.H. Topsoe, Appl. Catal. A 189 (1999) 205.
[5] S.T. Oyama, J. Catal. 216 (2003) 343.
[6] W. Li, B. Dhandapani, S.T. Oyama, Chem. Lett. 207 (1998).
[7] C. Stinner, R. Prins, Th. Weber, J. Catal. 191 (2000) 438.
[8] W.R.A.M. Robinson, J.N.M. van Gestel, T.I. Korányi, S. Eijsbouts, A.M. van der Kraan, J.A.R. van Veen, V.H.J. de Beer, J. Catal. 161 (1996) 539.
[9] D.C. Philips, S.J. Sawhill, R. Self, M.E. Bussell, J. Catal. 207 (2002) 266.
[10] S.J. Sawhill, D.C. Phillips, M.E. Bussell, J. Catal. 215 (2003) 208.
[11] S.T. Oyama, X. Wang, Y.K. Lee, K. Bando, F.G. Requejo, J. Catal. 210 (2002) 207.
[12] S.T. Oyama, X. Wang, Y.K. Lee, W.J. Chun, J. Catal. 221 (2004) 263.
[13] F. Sun, W. Wu, Z. Wu, J. Guo, Z. Wei, Y. Yang, Z. Jiang, F. Tian, C. Li, J. Catal. 228 (2004) 298.
[14] C. Stinner, Z. Tang, M. Haouas, Th. Weber, R. Prins, J. Catal. 208 (2002) 456.

[15] D.E.C. Corbridge, Studies in Inorganic Chemistry, vol. 10, fourth ed., Elsevier, Amsterdam, 1990.
[16] Y. Shu, S.T. Oyama, Chem. Commun. (2005) 1143.
[17] B.D. Cullity, Elements of X-Ray Diffraction, second ed., Addison–Wesley, Menlo Park, CA, 1978, p. 102.
[18] S. Ramanathan, S.T. Oyama, J. Phys. Chem. 99 (1995) 16365.
[19] S.J. Tauster, T.A. Pecoraro, R.R. Chianelli, J. Catal. 63 (1980) 515.
[20] X. Wang, P. Clark, S.T. Oyama, J. Catal. 208 (2002) 321.
[21] N. Hermann, M. Brorson, H. Topsoe, Catal. Lett. 65 (2000) 169.
[22] M. Egorova, R. Prins, J. Catal. 225 (2004) 417.
[23] S.K. Bej, S.K. Maity, U.T. Turaga, Energy Fuels 18 (5) (2004) 1227.
[24] K. Sakanishi, T. Nagamatsu, I. Mochida, D.D. Whitehurst, J. Mol. Catal. A 155 (2000) 101.
[25] J.M. Manoli, P.D. Costa, M. Brun, M. Vrinat, F. Maugé, C. Potvin, J. Catal. 221 (2004) 365.